# Modeling of 2D Axisymmetric Reacting Flow in Solid Rocket Motor with Preconditioning

*S. N. Lee* and S. W. Baek*[+]

** Ph.D. candidate, + Professor*
*School of Mechanical, Aerospace &Systems Engineering, Department of Aerospace Engineering, KAIST*
*373-1, Guseong-dong, Yuseong-gu, Daejeon 305-701, Korea*
*E-Mail: kirhi@kaist.ac.kr*

*Keywords : Solid Rocket, Precondition, AUSM, SST, Axisymmetric, Double Base, reaction*

**Abstract**

A numerical scheme for solid propellant rocket has been studied using preconditioning method to research unsteady combustion processes for the double-base propellant with a converging-diverging nozzle. The Navier-Stokes equation is solved by dual-time stepping method with finite volume method. The turbulence model uses a shear stress transport modeling. The species equation follows up the method of Xinping WI, Mridul Kumar and Kenneth K. Kuo. A preconditioned algorithm is applied to solve incompressible regime inside the combustor and compressible flow at nozzle. Mass flux was evaluated using modified advective upwind splitting method. The simulated result the comparison a fully coupled implicit method and a semi implicit method in terms of accuracy and efficiency. This report shows the result of solid rocket propellant combustion.

## 1. INTRODUCTION

For a long time, the solid rocket motors have been widely used for the application of military and civilian usage. None the less, the characteristic of reacting flow in solid rocket are so complicated that it is difficult to predict phenomena inside rockets quantitatively and qualitatively. T.S. Rho[1] analyzed the homogeneous propellant rocket with precon-ditioned method, but the result did not show a nozzle flow. Simulating a solid propellant combustion and nozzle flow affords valuable information that reveals physical and chemical processes inside rockets. The specified characteristics of solid rocket motor make the numerical algorithms less efficient. Whereas the regime of combustor is incompressible flow, nozzle flow is compressible. We need an algorithm that can be used for the entire range of flow speed to ensure accuracy and stiffness. In this problem, the preconditioning method made by Weiss[6] is applied to solve the entire reacting flow fields. A modified Advective Upwind Splitting Method(AUSM) method[10] is used to get mass flux in cell face. To make more exact analysis for turbulence behavior, modified Shear Stress Turbulence(SST) modeling[7] is used. A time marching integration is widely used in compressible flow, the numerical model is solved by dual-time stepping finite volume method.

## 2. SCHEMATIC OF SOLID ROCKET MOTOR

A schematic of solid rocket motor which is used in this simulation is shown in Figure 1.

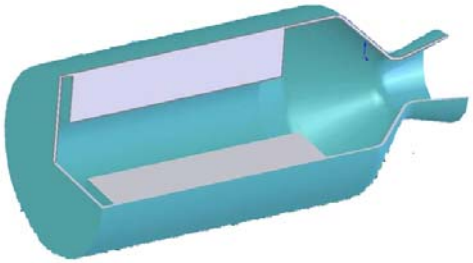

Fig. 1 Schematic of solid rocket motor

The chemical reaction step in the solid propellant rocket is quite complex, so it has difficult to collect an information of mechanism which is involved in the combustion process.

The combustion process is known for finishing after the five different reaction zones, which consist of preheat, foam, fizz, dark and luminous zones. The thickness is quite small, i.e. 300μm, so special care must be taken for grid generation and spacing. $NO_2$ and $CH_2O$ are selected as dominant species in the fizz zone. The other reaction zones are somewhat complex, which makes it difficult to decide species exactly. The present study employees a simplified model by Wu et al[3], i.e., including delayed reaction species 1,2(DR1,DR2) and product.

## 3. THEORETICAL FORMULATION

### 3.1 Governing Equation

A two dimensional axisymmetric solid rocket motor is examined here. The governing equations[6] for

the simulation of the rocket motor with a converging-diverging nozzle in Figure 1 are given in the following conservative forms.

$$\Gamma\frac{\partial Q_V}{\partial t}+\frac{\partial (E-E_V)}{\partial z}+\frac{\partial (F-F_V)}{\partial r}=\alpha H \qquad (1)$$

$$\Gamma=\begin{bmatrix} \rho_p & 0 & 0 & \rho_T & \rho_k & 0 & \rho_{Y_j} \\ u\rho_p & \rho & 0 & u\rho_T & u\rho_k & 0 & u\rho_{Y_j} \\ v\rho_p & 0 & \rho & v\rho_T & v\rho_k & 0 & v\rho_{Y_j} \\ H\rho_p-1 & \rho u & \rho v & H\rho_T+\rho c_p & \frac{5}{3}\rho+H\rho_k & 0 & \rho_{Y_j}+\rho H_{Y_j} \\ k\rho_p & 0 & 0 & k\rho_T & k\rho_k & 0 & k\rho_{Y_j} \\ w\rho_p & 0 & 0 & w\rho_T & w\rho_k & \rho & w\rho_{Y_j} \\ Y_i\rho_p & 0 & 0 & Y_i\rho_T & Y_i\rho_k & 0 & Y_i\rho_{Y_j}+\rho\delta_{ij} \end{bmatrix}$$

$$Q_v=\begin{pmatrix} p \\ u \\ v \\ T \\ k \\ w \\ Y_i \end{pmatrix}$$

This equation is converted from Eq. 2 which is not suitable for incompressible flow.

$\alpha$ is 1 for the axisymmetric flow and 0 for 2-d flow.

$$\frac{\partial Q}{\partial t}+\frac{\partial (E-E_V)}{\partial z}+\frac{\partial (F-F_V)}{\partial r}=\alpha H \qquad (2)$$

$$Q=\begin{pmatrix} \rho \\ \rho u \\ \rho v \\ \rho e \\ \rho k \\ \rho w \\ \rho Y_i \end{pmatrix} \quad E=\begin{pmatrix} \rho u \\ \rho u^2+p \\ \rho uv \\ \rho uH \\ \rho uk \\ \rho uw \\ \rho uY_i \end{pmatrix} \quad F=\begin{pmatrix} \rho v \\ \rho uv \\ \rho v^2+p \\ \rho vH \\ \rho vk \\ \rho vw \\ \rho vY_i \end{pmatrix}$$

$$E_V=\begin{pmatrix} 0 \\ \tau_{xx} \\ \tau_{xy} \\ u\tau_{xx}+v\tau_{xy}-q_x \\ \tau_{kx} \\ \tau_{wx} \\ q_{xi} \end{pmatrix} \quad F_V=\begin{pmatrix} 0 \\ \tau_{yx} \\ \tau_{yy} \\ u\tau_{yx}+v\tau_{yy}-q_y \\ \tau_{ky} \\ \tau_{wy} \\ q_{yi} \end{pmatrix}$$

$$H=\frac{1}{r}\begin{pmatrix} \rho v \\ \rho uv \\ \rho v^2 \\ \rho vH \\ \rho vk \\ \rho vw \\ \rho vY_i \end{pmatrix} \quad H_v=\frac{1}{r}\begin{pmatrix} 0 \\ \tau_{xy} \\ \tau_{yy}-\tau_{\theta\theta} \\ u\tau_{xy}+v\tau_{yy}-q_y \\ \tau_{ky} \\ \tau_{wy} \\ q_{yi} \end{pmatrix}$$

### 3.2 Physical Property

A thermal conductivity, viscosity and diffusion coefficient is calculated by Chapman-Enskog treatment.[12]

$$\eta=\frac{2.67\times10^{-6}(WT)^{\frac{1}{2}}}{\sigma^2\Omega_v} \qquad (3)$$

$$\lambda=(1.15+2.03/C_v/R)\eta/W\times C_v \qquad (4)$$

$$D_{jk}\left[\frac{m^2}{s}\right]=0.0188\frac{\sqrt{T^3/W_{jk}}}{p\sigma_{jk}^2\Omega_v} \qquad (5)$$

A couple of forms for the interaction coefficients in the conductivity and viscosity are useful and the following term is applied by Gordon et al.(1984)

$$\eta_{mix}=\sum_{i=1}^{Nm}\frac{x_i\eta_i}{x_i+\sum_{\substack{j=1\\ j\neq i}}^{Nm}x_j\phi_{ij}} \qquad (6)$$

$$\lambda_{mix}=\sum_{i=1}^{Nm}\frac{x_i\lambda_i}{x_i+\sum_{\substack{j=1\\ j\neq i}}^{Nm}x_j\varphi_{ij}} \qquad (7)$$

$$\phi_{ij}=\frac{1}{4}\left[1+\left(\frac{\eta_i}{\eta_j}\right)^{1/2}\left(\frac{M_j}{M_i}\right)^{1/4}\right]^2\left(\frac{2M_j}{M_i+M_j}\right)^{1/2} \qquad (8)$$

$$\varphi_{ij}=\phi_{ij}\left[1+\frac{2.41(M_i-M_j)(M_i-0.142M_j)}{(M_i+M_j)^2}\right] \qquad (9)$$

A mixture diffusion coefficient is defined by Wilke's mixing rule.[12]

$$D_{im}=(1-X_i)/\sum_{i\neq j}\frac{X_j}{D_{ij}} \qquad (10)$$

A heat capacity and enthalpy of species is based on polynomials of temperature by McBride et al.[11]

$$C_p^o(T)/R=a_1T^{-2}+a_2T^{-1}+a_3+a_4T+a_5T^2+a_6T^3+a_7T^4 \qquad (11)$$

$$H_p^o(T)/RT=-a_1T^{-2}+a_2\ln T/T+a_3+a_4T/2+a_5T^2/3+a_6T^3/4+a_7T^4/5+b1/T \qquad (12)$$

## 4. PRECONDITIONED DUAL-TIME STEPPING NAVIER-STOKES EQUATION

### 4.1 Fully-Implicit Method

Obtaining a solution by the whole matrix inversion in Eq. (1) is quite cumbersome since it takes a long computation time with increasing number of chemical species. However, it guaranties stiffness and accuracy of solution. To compare the result with another method, fully implicit method is applied first of all.

The algorithm is solved by LU-SGS Method.

$$\left[ D_i + \sum_j^{Nfaces} S_{jk} \right] \Delta Q = R_i^n \tag{13}$$

$$D_i = \Gamma + 1.5\frac{d\tau}{dt}\frac{\partial Q}{\partial Q_v} + \sum_j^{Nfaces} S_{ji} \tag{14}$$

$$S_{jk} = \left(\frac{\partial E_j - E_v}{\partial Q_{v,k}} + \frac{\partial F_j - F_v}{\partial Q_{v,k}}\right) \tag{15}$$

$$R_i = -\frac{3Q^{n+1} - 4Q^n + Q^{n-1}}{2} - \sum_j^{Nfaces} (E_j - E_v + F_j - F_v) \tag{16}$$

### 4.2 Semi-Implicit Method

Sometimes the computational time and efficiency is regarded as a more important thing if the result is similar. As the species is increase, the LU decomposition of matrix is more complicated and takes a long computation time. It is true that more efficient and faster to solve the equations separately. So, equation (2) is divided into three parts[14], Navier-Stokes equation, turbulent modeling, and reaction modeling. Each equation is treated using an implicit method.

$$\Gamma = \begin{bmatrix} \rho_p & 0 & 0 & \rho_t \\ u\rho_p & \rho & 0 & \rho_t \\ v\rho_p & 0 & \rho & \rho_t \\ H\rho_p - 1 & \rho u & \rho v & H\rho_t + \rho C_p \end{bmatrix} \tag{17}$$

$$\Gamma_r = \begin{bmatrix} \rho & 0 & 0 & 0 \\ 0 & \rho & 0 & 0 \\ 0 & 0 & \rho & 0 \\ 0 & 0 & 0 & \rho \end{bmatrix} \tag{18}$$

The source term which is made by semi-implicit method is transformed by following procedure.

$$D_c = -\frac{1}{\beta}\frac{\partial P}{\partial \tau}\begin{bmatrix} k \\ w \end{bmatrix} \tag{19}$$

$$D_c = -\frac{1}{\beta}\frac{\partial P}{\partial \tau}\begin{bmatrix} Y_1 \\ Y_2 \\ Y_3 \\ Y_4 \\ \vdots \end{bmatrix} \tag{20}$$

### 4.3 Finite Volume Method

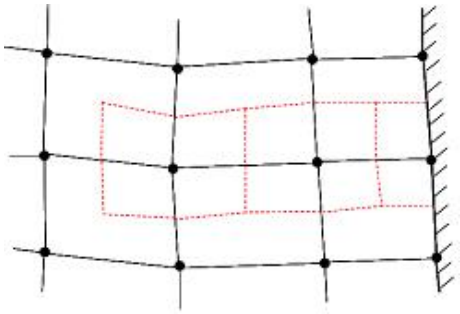

Fig. 2 FVM Grid

Vertex/Solutions ●
Grid Lines –
Boundary ″
Cell-edges -----

An algorithm is developed by finite volume method. The grid is not transformed into the computational domain. Each grid point has information of surface vector so that normal velocity can be stored for mass flux.

The chemical reaction procedures end within a 300μm from solid propellant surface[1]. To find accurate reaction zone, grid generation is very important. Here the minimum grid size is 0.7μm

$$\frac{\partial}{\partial t}\int_\Omega U d\Omega + \int_\Gamma (Fdr - Gdx) = \int_\Gamma (Rdr - Sdx) - \int_\Omega H d\Omega \tag{21}$$

$$\begin{aligned} &D_{i,j}\Delta Q_{i,j} + A_{i,j}\Delta Q_{i-1,j} + B_{i,j}\Delta Q_{i,j-1} \\ &+C_{i,j}\Delta Q_{i+1,j} + E_{i,j}\Delta Q_{i,j+1} = -R_{i,j} \end{aligned} \tag{22}$$

### 4.4 Advective Upwind Splitting Method

Liou's AUSM+(P)[10] is applied for the cell face mass flux and pressure.

$$E = \rho u_{\frac{1}{2}} \begin{bmatrix} 1 \\ u \\ v \\ H \end{bmatrix}, E_p = \begin{bmatrix} 0 \\ p_{\frac{1}{2}} \\ 0 \\ 0 \end{bmatrix} \tag{23}$$

$$M_i = u_i / a_{\frac{1}{2}} \tag{24}$$

$$M_{(1)}^{\pm} = \frac{1}{2}(M \pm |M|) \tag{25}$$

$$M_{(4)}^{\pm} = \begin{Bmatrix} \pm\frac{1}{4}(M \pm 1)^2 \pm \frac{1}{8}(M^2 - 1)^2 \\ M_{(1)}^{\pm} \end{Bmatrix} \begin{Bmatrix} \|M\| < 1 \end{Bmatrix} \tag{26}$$

$$P_{(5)}^{\pm} = \begin{Bmatrix} \frac{1}{4}(M \pm 1)^2(2 \mp M) \pm \frac{1}{16}M(M^2 - 1)^2 \\ (1/M)M_{(1)}^{\pm} \end{Bmatrix} \begin{Bmatrix} \|M\| < 1 \end{Bmatrix} \tag{27}$$

### 4.5 Shear Stress Turbulence Model

The κ-ω turbulence modeling is known for accurate method near wall boundary, but in the free stream region, its results do not match experimental observations well. To get more exact solution, a shear stress turbulence (SST)[7] modeling introduced in this report. It obeys κ-ω source term near the wall and the κ-ε controls production-dissipation term in free stream

$$\frac{\partial \rho k}{\partial t}+\frac{\partial \rho uk}{\partial z}+\frac{\partial \rho vk}{\partial r}=\frac{\partial}{\partial z}(\mu_l+\mu_t/\sigma_k)\frac{\partial k}{\partial z}+\frac{\partial}{\partial r}(\mu_l+\mu_t/\sigma_k)\frac{\partial k}{\partial r}+H+S \tag{28}$$

$$\frac{\partial \rho \omega}{\partial t}+\frac{\partial \rho u\omega}{\partial z}+\frac{\partial \rho v\omega}{\partial r}=\frac{\partial}{\partial z}(\mu_l+\mu_t/\sigma_k)\frac{\partial \omega}{\partial z}+\frac{\partial}{\partial r}(\mu_l+\mu_t/\sigma_k)\frac{\partial \omega}{\partial r}+H+S \tag{29}$$

In case of SST model, the term is called by F1 is drawn to control near wall and free stream.

$$F_1=TANH(\arg_1^4) \tag{30}$$

$$\arg_1=\min[\max(\frac{\sqrt{k}}{0.09\omega r},\frac{500\nu}{\omega r^2}),\frac{4\rho\sigma_{w2}k}{CD_{kw}r^2}] \tag{31}$$

$$CD_{kw}=\max[2\rho\sigma_{w2}\frac{1}{\omega}\frac{\partial k}{\partial z_i}\frac{\partial \omega}{\partial z_i},10^{-20}] \tag{32}$$

Compressible effect is dominant in supersonic region. As a result, the low Reynolds turbulence model does not show turbulence effect in algorithm. Sakar modified turbulence algorithms to validate in supersonic region.

### 4.6 Reaction Model

In this problem, Double base solid propellant is used for chemical combustion. The reaction of solid propellant is quite complex. Wu, X.[3] introduced simplified reaction mechanism by following equation.

$$5CH_2O+7NO_2\rightarrow 7NO+5H_2O+3CO+2CO_2 \tag{33}$$

The chemical source terms in the species equation are represented below equation.

$$\overline{\dot{w}}_{F,ch}=-A_{fz}\exp(-E_{a,fz}/R_u\tilde{T})\overline{\rho}^2\tilde{Y}_F\tilde{Y}_o/W_O \tag{34}$$

$$\overline{\dot{w}}_{DR1,ch}=-A_{DR1}\exp(-E_{a,DR1}/R_u\tilde{T})\overline{\rho}^2\tilde{Y}_{DR1}{}^2/W_{DR1} \tag{35}$$

$$\overline{\dot{w}}_{DR2,ch}=-A_{DR2}\exp(-E_{a,DR2}/R_u\tilde{T})\overline{\rho}^2\tilde{Y}_{DR2}{}^2/W_{DR2} -(1+v_oW_o/v_FW_F)\overline{\dot{w}}_F \tag{36}$$

Surface regression rate follows up an Arrhenius type.

$$r=-4.12\exp(-35.3/R_u\tilde{T}) \tag{37}$$

### 4.7 Boundary Condition

No-slip, zero gradients for pressure, temperature and species condition is used for wall condition. In axisymmetric line, Neumann condition is used. Supersonic outlet has

$$v_1=0\ ,\ \frac{\partial \phi_1}{\partial r_1}=0 \tag{38}$$

$$\phi_{\mathrm{lm}}=\phi_{\mathrm{lm}-1} \tag{39}$$

ϕ indicate physical properties like pressure, temperature, velocity.

Turbulence wall boundary condition is followed.

$$\begin{aligned} k&=0\\ w&=60\mu/\rho/0.075/y_{wall}{}^2 \end{aligned} \tag{40}$$

Free stream boundary condition is specified.

$$\begin{aligned} w_{free}&=10V_{free}/l\\ k_{free}&=0.01\mu w_{free}/\rho \end{aligned} \tag{41}$$

Mass conservation is user for solid propellant surface.

$$\rho vY_i=\rho_s r_b Y_{i,s}+\rho D_f\frac{\partial Y}{\partial r} \tag{42}$$

Propellant surface temperature is drawn out from energy equation and pressure is deduced from momentum balance. The properties of homogeneous propellant used in this simulation are in the table 1.

Table 1 Properties of DBSP : Solid and Gas

| | $DBSP_s$ | $DBSP_g$ |
|---|---|---|
| Density, kg/m$^3$ | 1600 | // |
| Rgas | // | 8.314e3J/kmol |
| $pr_t$ | // | 0.9 |
| $A_f$, m$^3$/kmol | | 1.e7 |
| $A_{dr1}$, m$^3$/kmol | | 1.e10 |
| $A_{dr2}$, m$^3$/kmol | | 1.e10 |
| $E_f$, kJ/mol | | 33.5 |
| $E_{dr1}$, kJ/mol | | 209 |
| $E_{dr2}$, kJ/mol | | 209 |
| $W_f$, kg/kmol | | 30.03 |
| $W_o$, kg/kmol | | 46.01 |
| $W_{dr1}$, kg/kmol | | 27.78 |
| $W_{dr2}$, kg/kmol | | 27.78 |

## 5. NUMERICAL VALIDATION

To confirm the code, some cases are validated. One is JPL nozzle flow. Inlet condition is 1Mpa and 1000k. Initial condition is 100Kpa and 298k. Comparing with experimental result in Figure 4, it has very similar value.

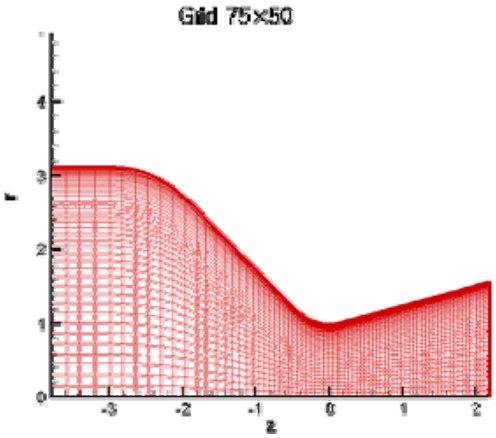


Fig. 3 JPL NOZZLE

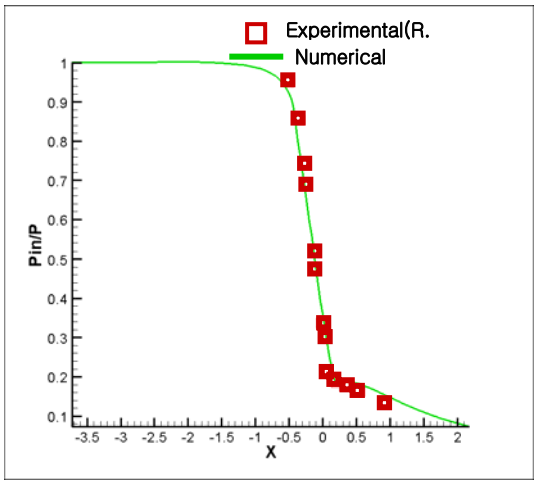


Fig. 4 WALL PRESSURE

To validate turbulence modeling, Wilcox's[13] data is compared for 13,750 Reynolds number. It is fully developed flow. Without turbulence modeling in Figure 6, it shows significant difference.

The code in this report quite matches well both supersonic region and subsonic area.

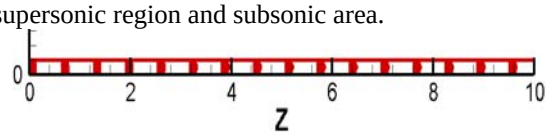


Fig. 5 FULLY DEVELOPED CHANNEL

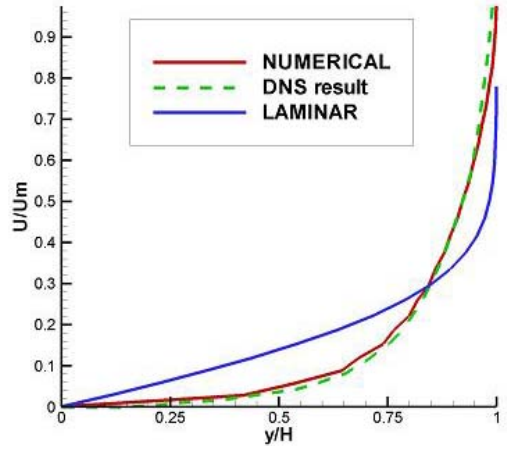


Fig. 6 NUMERICAL vs. DNS

## 6. NUMERICAL RESULT

In order to show the quantitative physical property at each time dual time is applied in the algorithms.

Following Figure 7 is generated to calculate the solid propellant combustion which is attached to the solid rocket motor.

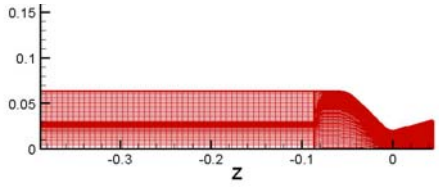


Fig. 7 GRID GENERATION

Figure 8 shows the species profile from solid propellant space. A fuel decreases as the location is increased and DR2 species is gradually increasing but decreases again after making product species, i.e. flame temperature.

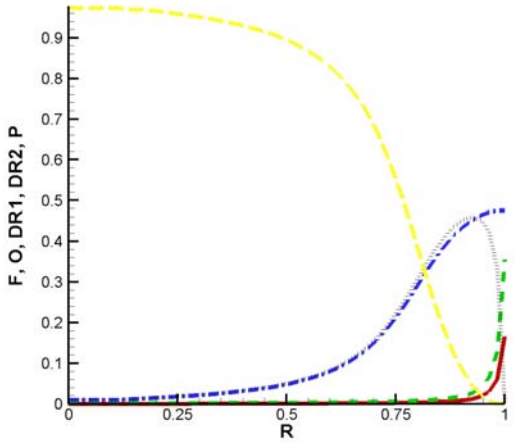


Fig. 8 SPECIES DISTRIBUTION

Below velocity vector in Figure 9 inform the vortex region due to interaction of nozzle wall and solid propellant. Without the propellant in a combustor, there is no vortex, and it is a different with real solid rocket reaction. Because it makes some problem that do not react near solid propellant surface well.

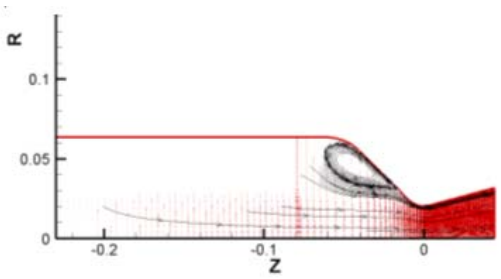


Fig. 9 STREAM LINE

Figure 10, 11 point out that fully implicit method and semi-implicit method have a little difference. Green indicate fully implicit method and black or red one figure out semi-implicit result.

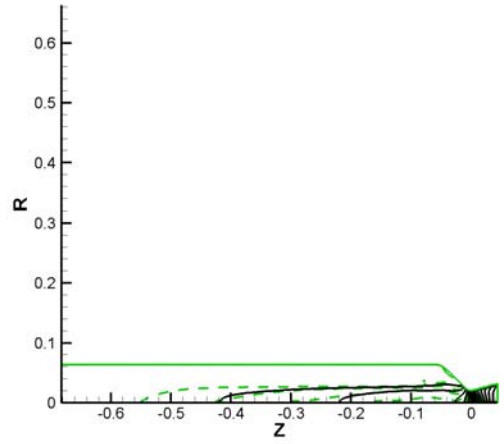


Fig. 10 MACH CONTOUR (FULL vs. SEMI)

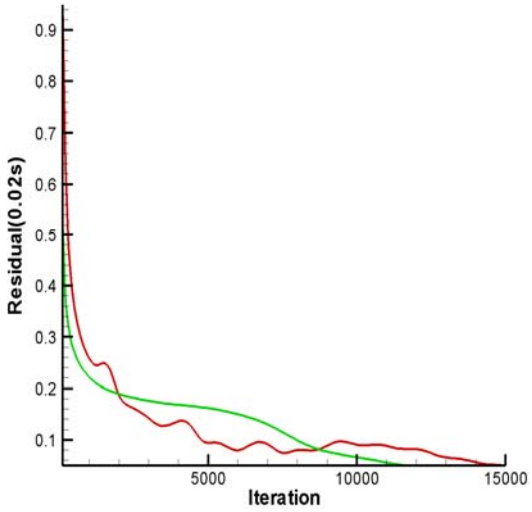


Fig. 11 RESIDUAL (FULLY vs. SEMI)

## CONCLUSION

In case of steady state solution, CPU time was 6735 for Semi-Implicit and 12586 for Fully-Implicit Method. There is numerical fluctuation for the Semi-Implicit method during the iteration. The computation time is much slower as species increase in case of fully implicit method. However, in terms of the Numerical result, they are very similar. To simulate real rocket motor performance, solid propellant attached combustor wall. The semi-implicit one has more efficient and faster solutions and can figure out real phenomenon in rocket motor.

## Acknowledgments

This work was supported by grant of Agency for Defense Development.

## References

1) T. S. Roh, I-S Tseng and V. Yang, "Effects of Acoustic Oscillations on Flame Dynamics of Homogeneous Propellants in Rocket Motors," *Journal of Propulsion and Power*, Vol. 11, No. 4, pp. 640-650, 1995.
2) I. S. Tseng and V. Yang, "Combustion of a Double-Base Homogeneous Propellant in a Rocket Motor," *Combustion and Flame*, Vol. 96, pp. 325-342, 1994.
3) X. WU. M. Kumar and K. K. Kuo, "A Comprehensive Erosive-Burning Model for Double-Base Propellants in Strong Turbulent Shear Flow," *Combustion and Flame*, Vol. 53, pp. 49-63, 1983.
4) J.M.Weiss and W.A.Smith, 1994 "Preconditioning Applied to Variable and Constant Density Time-Accurate Flows on Unstructured Meshes." *AIAA paper* 94-2209. 1994
5) J. R. Edwards, "Low-Diffusion Flux-Splitting Methods for Flows at All Speeds." *AIAA Journal*, Vol. 36, No. 9, 1998
6) J. M. Weiss, J. P. maruszewski, and W. A. Smith, "Implicit Solution of Preconditioned Navier-Stokes Equations Using Algebraic Multigrid." *AIAA Journal*, Vol. 37, No. 1, 1999
7) S. H. Park and J. H. Kwon, "Implementation of k-w Turbulence Models in an Implicit Multigrid Method." *AIAA Journal*, Vol. 42, No. 7, 2004
8) F. Liu and X. Zheng, "A Strongly Coupled Time-Marching Method for Solving the Navier-Stokes and k-w Turbulence Model Equation with Multigrid." *J. Computational Physics*, 128, 289-300. 1996
9) J.-S. Shuen, K.-H. Chen and Y. Choi, "A Coupled Implicit Method for Chemical Non-equilibrium Flows at All Speeds." *J. Computational Physics*, 106, 306-318. 1993
10) M.S. Liou, "A sequel to AUSM, Part II : AUSM+ - up for All Speeds", *J. Computational Physics*, 214, 137-170. 2006
11) M. J. Zehe, S. Gordon and B. J. McBride, "CAP : A Computer Code for Generating Tabular Thermodynamic Functions from NASA Lewis Coefficient", NASA/TP-2001-210959, 2002
12) B. E. Poling, J. M. Prausnitz and J. P. O'Connell, *The Properties of Gases and Liquids*, McGRAW-HILL, 5th Edition.
13) Wilcox, David C., Turbulence Modeling for CFD, DCW Industries, 2th Edition.
14) K.H. Chen, D. Fricker, J. Lee and J. Moder, ALLSPD -3D User Guide, Turbomachinery and Propulsion System Division, NASA Lewis Research Center, 1998